Catal Lett (2012) 142:1312–1320
DOI 10.1007/s10562-012-0900-7

Effect of Activation Method on the HDS Activity of Unsupported CoMoS Catalysts Prepared from a Novel Precursor

F. Niefind · J. Cruz-Reyes · M. Del Valle · L. Kienle · A. Lotnik · G. Alonso-Nunez · M. Armbrüster · W. Bensch

Received: 26 April 2012 / Accepted: 28 August 2012 / Published online: 18 September 2012

Abstract Unsupported Co promoted MoS_2 catalysts for the hydrodesulfurization (HDS) reaction were prepared using a mixture of $Co(dien)_2MoS_4$ (dien = diethylenetriamine) and tetrapropylammonium thiomolybdate. The mixture was first treated in a high energy ball mill followed either by ex situ activation in forming gas or by in situ activation during the HDS reaction. The ex situ activation mode leads to a very active catalyst exhibiting 84.9 % conversion of dibenzothiophene within 5 h. The in situ activated catalyst is less active but still shows a remarkable performance. Transmission microscopy investigation demonstrates that in the ex situ activated catalyst the stacking of MoS_2 slabs is lower than in the in situ obtained material, which is corroborated by Raman measurements on the materials. In addition, the average MoS_2 slab length of the former sample is significantly shorter than for the latter material. During the in situ activation, crystalline Co_9S_8 is formed which may be a reason for the lower HDS activity. The chemical composition of the two catalysts is also different, with larger carbon and sulfur contents found for the in situ-formed sample. The deposition of carbon and sulfur on the surface of the catalyst may also account for the lower catalytic activity, compared to the ex situ obtained material.

Keywords Hydrodesulfurization · Unsupported CoMoS · Activation method

F. Niefind · W. Bensch (✉)
Institute for Inorganic Chemistry, University of Kiel, Max-Eyth-Str. 2, 24118 Kiel, Germany
e-mail: wbensch@ac.uni-kiel.de

J. Cruz-Reyes · M. Del Valle
Facultad de Ciencias Químicas e Ingeniería, UABC, Tijuana, Baja California, Mexico

L. Kienle · A. Lotnik
Synthesis and Real Structure of Solids, Technical Faculty, University of Kiel, Kaiserstr. 2, 24143 Kiel, Germany

G. Alonso-Nunez
Centro de Nanociencias y Nanotecnologia, Universidad Nacional Autónoma de México, C.P. 22860 Ensenada, Baja California, Mexico

M. Armbrüster
Max-Planck-Institut für Chemische Physik fester Stoffe, Nöthnitzer Str. 40, 01187 Dresden, Germany

1 Introduction

For the reduction of SO_x emissions produced during combustion of mineral oil products, sulfur concentration must be reduced and the 10 ppm level is now standard in many countries in the world [1–3]. The desulfurization of refinery streams is achieved at elevated temperatures by using hydrogen, and MoS_2-based catalysts which are either promoted by Co or by Ni. The preparation of the catalysts is normally performed using oxidic precursors like ammonium heptamolybdate and suitable Ni and Co salts. By introducing defects, the Ni or Co promoter increases the structural disorder of MoS_2, yielding highly active MoS_2 species [4, 5]. The synergism between Co/Ni and Mo has been mostly attributed to an electronic effect [6, 7]. An important but not fully understood role is ascribed to carbon within or on the catalyst surface. Some studies have suggested that carbon is directly involved in the desulfurization reaction [8–10]. According to recent results β-Mo_2C is formed in situ on the surface of the catalyst under HDS conditions, while regions near the surface are transformed into MoS_xC_y [11]. Relatively large

specific surface areas were reported for catalysts prepared from organic ammonium thiomolybdates [12, 13]. During the last few years we have developed a different route for the preparation of HDS catalysts, avoiding the use of oxidic Mo precursors [14–18]. Applying Mo–S containing sources should allow complete sulfidization at relatively low temperatures which was demonstrated in detailed differential thermal analysis studies [19]. The catalysts prepared with sulfur-containing Mo sources were also promoted with Co or Ni using thiocarbamate complexes which decompose at a temperature similar to that of the Mo thiocompounds, thus preventing segregation of Co or Ni sulfides. All catalysts exhibited a good performance in the HDS reaction, with activities comparable or even better than commercially available γ-Al_2O_3 supported catalysts. Interestingly, most catalysts did not consist of MoS_2 single layers but rather of stacks of 5–7 MoS_2 layers [14–18, 20]. The high activity was explained on the basis of a large concentration of coordinatively unsaturated sites created during the decomposition process. In addition, depending on the carbon content in the precursor material, the in situ decomposition of tetraalkylammonium thiomolybdates yields unsupported Mo sulfide catalysts which are often characterized by high surface areas and improved catalytic activity in the HDS of dibenzothiophene (DBT). A possible explanation for the improved catalytic properties of such materials proposes a partial substitution of sulfur atoms by carbon, generating systems like $MoS_{2-x}C_y$ [11, 21–23].

Very recently $[RN(CH_3)_3]_2MoS_4$ (R = lauryl, myristyl or cetyl) precursors were in situ decomposed yielding catalysts with specific surface area of more than 400 m^2/g and high DBT conversion rates [24]. The Mo:S ratio in these catalysts was close to 2 and depending on R, C:Mo reached the very large value of 6.5. In our ongoing work we used mixtures of two different Mo sources, namely $Co(dien)_2MoS_4$ and tetrapropylammonium-thiomolybdate (TPATM), which were thermally decomposed yielding $CoMoS_x$ catalysts. In this work, $Co(dien)_2MoS_4$ (dien = diethylenetriamine) TPATM and were synthesized and used as catalyst precursors; the properties in the HDS reaction and the microstructure of the unsupported catalysts are presented. The effects of in situ and ex situ activation of the catalysts onto the properties and HDS activity are also discussed.

2 Experimental Details

The precursor $Co(dien)_2MoS_4$ ($Co(dien)_2TM$) was prepared using ammonium thiomolybdate (ATM), cobalt acetate tetra hydrate $Co(OAc)_2{\cdot}4H_2O$ and diethylenetriamine (*dien*). First an aqueous solution (40 mL) was prepared of 3.49 g (14 mmol) of $Co(OAc)_2{\cdot}4H_2O$ and then 3.025 mL of *dien* (28 mmol) were added. ATM (3.65 g, 14 mmol) was dissolved in 120 mL·H_2O and this solution was added to the first solution. A red-brown precipitate was formed immediately which was filtered off and dried in vacuum. The yield was about 97 %. The precursor TPATM was synthesized mixing a solution of 4.23 g (106 mmol) NaOH dissolved in 50 mL with 18.75 g (59.2 mmol) tetrapropylammonium bromide. This solution was then mixed with 8.89 g (34.3 mmol) ATM dissolved in 176 mL H_2O. The red precipitate was filtered off and washed with a small amount of ethanol. In accordance with literature data the yield was about 80 % [19]. The two precursors $Co(dien)_2TM$ and TPATM were mixed in a molar ratio Co/(Co + Mo) = 0.4 and treated in a ball mill for 1 h in Argon atmosphere [14]. One half of the mixture was directly used in the HDS reaction of DBT without further treatment (sample name: CoMoS-A, in situ activated). The other half of the resulting mixture was heated in a flow of forming gas (1.4 L min^{-1} flow rate, with a ratio H_2/N_2 (10 % of H_2), in a rotating oven (500 rpm) at 350 °C for 2 h. The heating and cooling rates were 100 °C/h (Sample name: CoMoS-B, ex situ activated).

X-ray powder patterns were recorded with a STOE STADI-P instrument (monochromatized CuK∝1 radiation, $\lambda = 1.54056$ Å) in transmission mode with a position sensitive detector. Chemical elemental analyses were performed with a EURO Vector EA Combustion analyzer using zinc sample holder. The samples were heated up to 1,000 °C under oxygen atmosphere and the gases were detected by a thermal conductivity cell.

Measurements of the Raman spectra were taken following a fixed protocol for all three samples. After selecting a spot for the measurements, laser light with 514 nm was attenuated to 10 mW and focused on the sample via a 50× objective (Labram 010 spectrometer, Jobin-Yvon). Subsequently, four spectra as described below were recorded in the range of 0–4,200 cm^{-1} consisting of 20 single spectra in five different Raman regions: (i) 10 mW, accumulation time 300 s, total measurement time 8.5 h; (ii) 100 mW, accumulation time 30 s, total measurement time 50 min; (iii) 10 mW, accumulation time 300 s, total measurement time 8.5 h; (iv) 100 mW, accumulation time 30 s, total measurement time 50 min.

After these measurements, a new spot was selected to ensure reproducibility of spectra obtained in (i) This measurement protocol allows differentiating between reversible and irreversible laser damage in the samples, which turned out to be crucial to record spectra of the materials.

Nitrogen adsorption measurements were carried out at 77 K on a Quantachrom Autosorb-1. Samples were degassed under flowing argon at 473 K for 2 h before N_2 adsorption. The BET surface areas were calculated from $p/p_0 = 0.03$–0.3 in the adsorption branch.

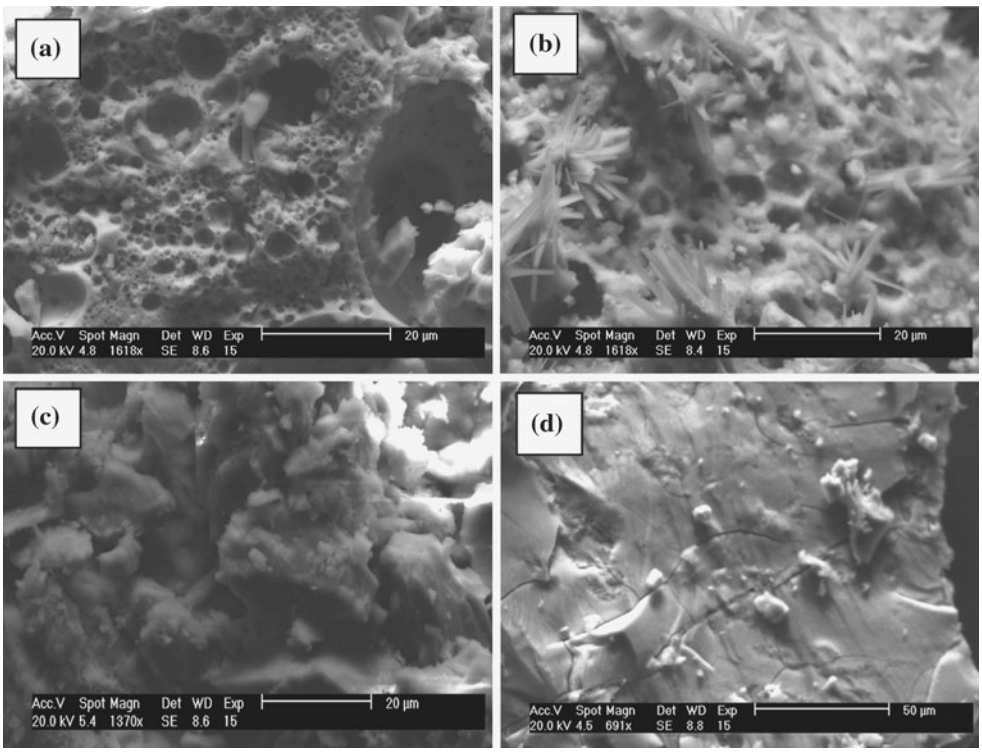

Fig. 1 SEM images of the catalyst CoMoS-A obtained by in situ (**a**, **b**) and CoMoS-B obtained by ex situ (**c**, **d**) treatment

Table 1 Chemical composition of the catalysts determined with CHNS analyses

Sample	%N	%C	%H	%S	Mo	S	C
CoMoS-A after HDS	1.28	15.31	2.22	34.0	1.0	3.04	3.65
CoMoS-B after HDS	2.52	9.46	0.91	31.0	1.0	2.33	1.89
CoMoS-B before HDS	2.69	7.14	1.19	31.3	1.0	2.28	1.39

Transmission Electron Microscopy (TEM) investigations were performed with a Tecnai 30 STwin microscope (300 kV, FEG cathode, $C_S = 1.2$ mm). The samples for TEM investigations were prepared as follows. Small amount of powder containing mesoporous MoS_2 was suspended in methanol and ultrasonically grinded for 15 min. Afterwards, a transfer of the suspended powder on a TEM support (a lacey carbon film on 200 mesh copper grid) was carried out by dipping of the TEM support into the solution. The prepared TEM samples were dried at a room temperature for several minutes. All images were recorded with a Gatan Multiscan CCD camera (2k×2k) and evaluated (including Fourier analyses) with a program Digital Micrograph (Gatan). EDS analyses were performed in the TEM mode with a Si/Li detector (EDAX System).

The HDS of DBT was tested in a high pressure 300 mL Parr reactor by placing 4.4 g DBT, 100 mL of decalin and 0.300 g of the catalyst applied in the as-prepared state. The reactor was purged of residual air, pressurized with H_2 to 3.1 MPa (450 psi) and then heated to the reaction temperature of 623 K in about 10 min. A stirring rate of 600 rpm was used. The progress of the reaction was monitored by gas chromatography with a HP 6890 gas chromatograph, using samples taken every 20 min. During the first hour, then every 30 min for the next 4 h. Reduction of the sample volume due to sampling was ≤5 % of total volume. The identity of the reaction products was confirmed by mass spectrometry with a HP 6890 GC–MS, using a HP-5MS capillary column (30 m × 0.25 mm × 0.25 µm). The catalytic activity is expressed in terms of percentage conversion of DBT vs. reaction time, and from these data, the reaction rates were calculated for each catalyst. The mean standard deviation for catalytic measurements was about 2.5 %. The HDS of DBT yields biphenyl (BP) through the direct desulfurization pathway (DDS), and tetrahydrodibenzothiophene (THDBT) through the hydrogenation pathway (HYD). Since these two pathways are parallel [26], the selectivity ratio (HYD)/(DDS) was calculated by the equation:

$$\mathrm{HYD/DDS} = [\mathrm{THDBT}]/[\mathrm{BP}] \quad (1)$$

3 Results and Discussion

In the structure of the precursor $Co(dien)_2MoS_4$ the Co^{2+} cation is chelated in an octahedral environment by two tridentate acting *dien* ligands and Mo^{6+} is in a tetrahedral surrounding of S^{2-} anions. Hence, the two components are not covalently bound.

The specific surface areas of CoMoS-A and CoMoS-B of 2.4 and 3.5 m^2g^{-1} respectively are smaller than those reported for other unsupported CoMo sulfide catalysts [25].

The SEM images of the two samples are displayed in Fig. 1. While the catalyst obtained by in situ activation exhibits a sponge-like morphology with 'craters' of different diameters, the catalysts prepared with ex situ activation appears as more dense material and with small crystallites in the μm range located on the surface. In some regions of the in situ treated material small needle-like crystals are seen (Fig. 1, top right) which are Co rich.

The results of the chemical analyses of the two catalysts are summarized in Table 1. There are several remarkable differences between the two catalysts. The CoMoS-A catalyst contains a much higher C and H content than the CoMoS-B catalyst. It is also obvious from the data that the S and N contents of the catalyst CoMoS-B are only slightly affected by the HDS test reaction.

The X-ray powder patterns of the catalysts before and after the HDS reaction are displayed in Fig. 2. As can be seen, the as-prepared material is microcrystalline (Fig. 1, top, red trace) and after the in situ treatment during the HDS test all reflections disappeared and a typical diffraction pattern of a nanosized material exhibiting a strong disorder and low stacking is obtained [27–29]. Only broad modulations are seen near the (100), (101) and (110) reflections, which are associated with materials with low crystallinity. The asymmetric shape of the (100) reflection additionally indicates layers that are randomly rotated against each other [29].

All patterns are also characterized by diffuse scattering in the region of the (002) reflection being caused by unstacked layers. In addition, the (002) reflection is absent in all patterns and according to literature [11, 29] this observation points to a high dispersion of the slabs and to nanometric scale particles as discussed by several authors who have synthesized MoS_2 [29, 30]. All observations in the X-ray powder patterns are clear indications of a low stacking of MoS_2 layers in the materials. In addition, no hints are found for crystalline CoS_x phases like Co_9S_8, $CoS_{1.03}$ or $CoS_{1.09}$ [31, 32] indicating suppression of phase separation and pointing to a very good dispersion of Co.

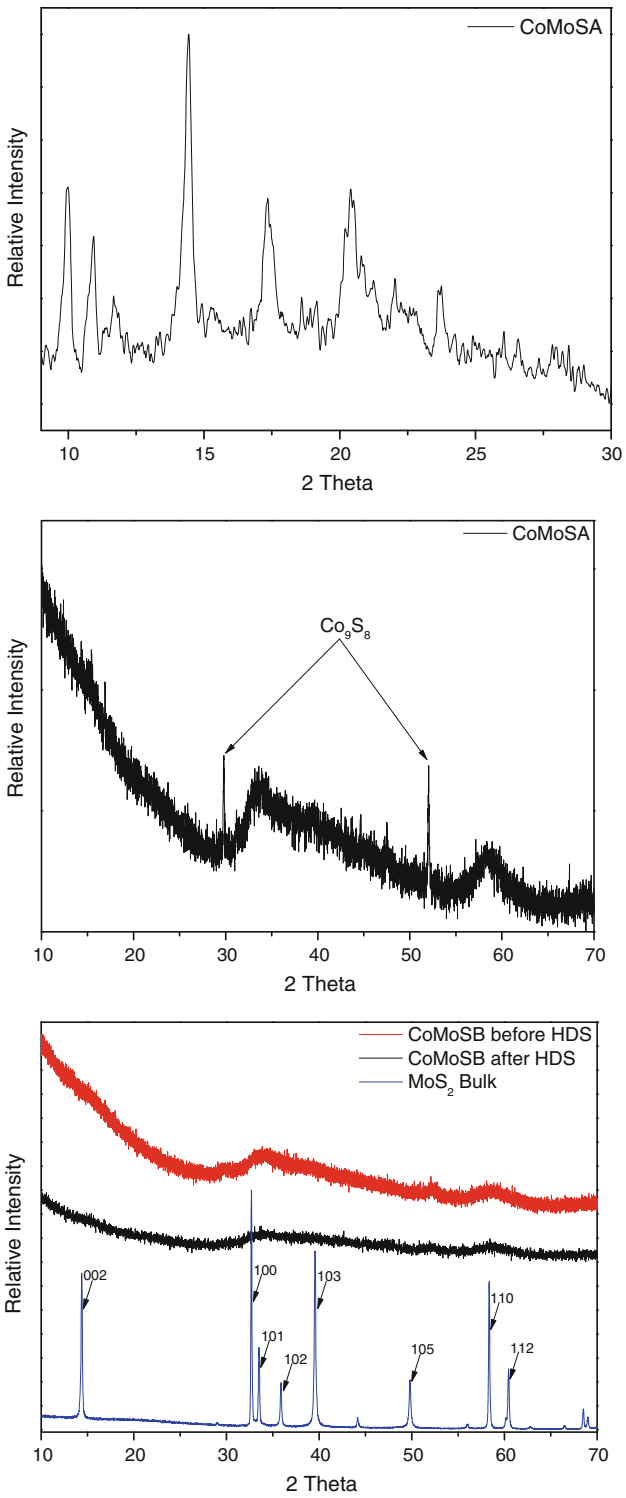

Fig. 2 X-ray powder patterns of the catalysts before and after the HDS test reaction. *Top*: The catalyst in the as-prepared state; *middle*: the pattern after the HDS test reaction. Note the occurrence of reflections of Co_9S_8; *bottom*: ex situ activated catalyst before HDS (*red pattern*) and after the reaction (*black line*). The powder pattern of a polycrystalline MoS_2 sample is provided for comparison (*blue pattern*)

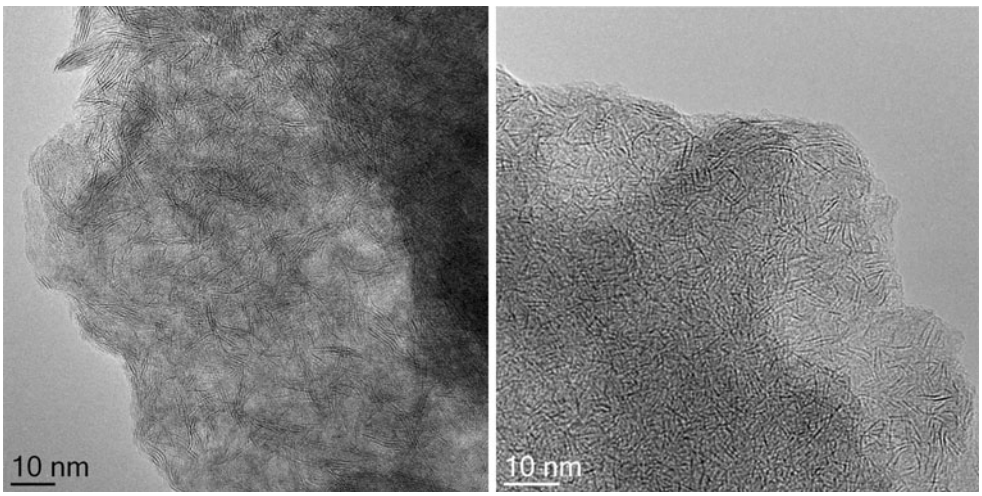

Fig. 3 TEM micrographs of the catalysts after the HDS test reactions. *Left*: in situ activated; *right*: ex situ activated materials

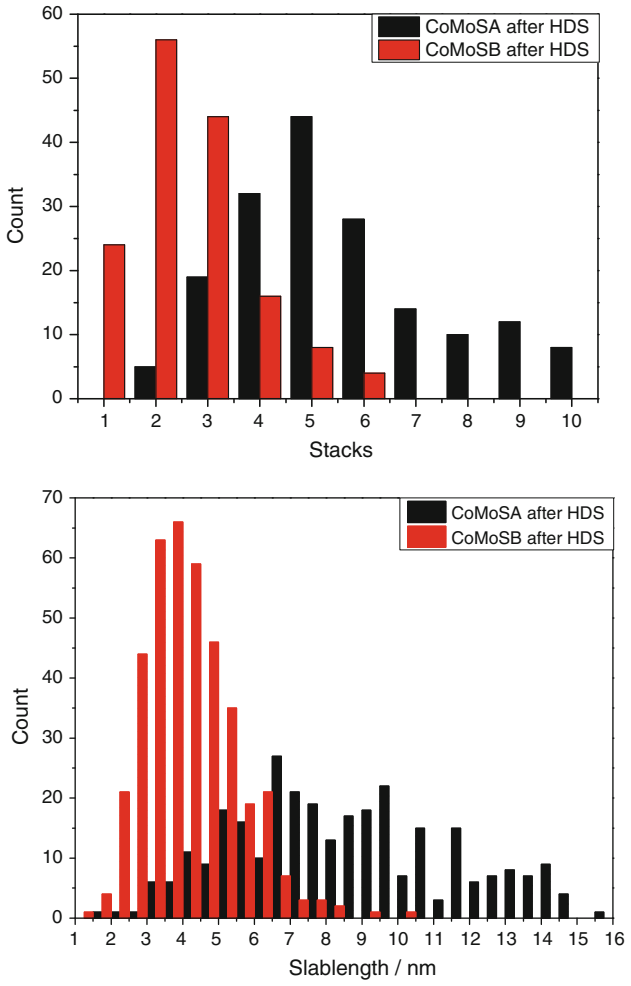

Fig. 4 Statistical evaluation of the stacking (*top*) and the layers lengths (*bottom*) in the two catalysts

For the ex situ activated material the differences of the powder patterns before and after the HDS test are small. A slightly decreased intensity of the (100), (101) and (110) reflections are seen in the pattern of the ex situ activated catalyst after the HDS treatment suggesting that the layers are displaced against each other like a spread deck of cards.

The pattern of the in situ activated material after the HDS reaction exhibits reflections of crystalline Co_9S_8 indicating a phase separation during the reaction. But the overall pattern reflects a low crystallinity of the material. In contrast to the in situ activated material, no hints are found for a phase separation in the material prepared by the ex situ method. The destacking phenomenon has been reported in literature in catalytic systems where thiomolybdate precursors with alkyl groups have been used, indicating that carbon has an outstanding influence on the dispersion of the (002) planes [33, 34]. This effect was ascribed to an initial bending of the slabs induced by the replacement of sulfur edge atoms by structural carbon [11].

In the HREM micrographs (Fig. 3) the (002) planes exhibit a *d* spacing of 0.62 nm. For both samples investigated after the HDS reaction the catalysts are characterized by short layers and a low stacking number. Moreover, many layers are bent and defects can clearly be detected. Many MoS_2 nanoparticles exhibit a random orientation to each other. Whereas for the in situ activated catalyst, stacking numbers up to about 10 are apparent (see Fig. 4), the situation is different for the ex situ activated material with a much lower average stacking number with most particles exhibiting 1–3 slabs. This fact underscores the high dispersion of the material. The average lengths of the MoS_2 layers differ as well. On average shorter layers are observed for the ex situ activated material, with most particles displaying a length between 3 and 13 nm. For the in situ activated catalyst a broad distribution is found from about 3–19 nm (Fig. 4). The XRD and TEM results clearly demonstrate the significant influence of the treatment applied to decompose the precursor on the microstructure of the catalysts. In the in situ method, the atmosphere

provided by the H_2/H_2S mixture seems to help to partially restore the atomic layers of MoS_2.

The nanosized nature of the catalysts is also evident in the Raman spectra (Fig. 5). Generally, Raman spectroscopy is widely used to analyze bulk and nanosized MoS_2 particles of different shapes and sizes [35–41]. The energetic positions of the two bands E^1_{2g} and A_{1g} are indicators of the slab stacking. The A_{1g} mode which is located at 411 cm^{-1} in bulk material (Fig. 5, bottom) shifts to lower wave numbers when the number of stacked MoS_2 slabs is reduced and is observed at 398 cm^{-1} (Fig. 5, top) for the ex situ activated material, i.e. a shift of 13 cm^{-1} is observed. The E^1_{2g} mode is less sensitive and exhibits a smaller downward shift of about 10 cm^{-1} from 386 cm^{-1} (bulk) to 376 cm^{-1}. For the in situ activated material (Fig. 5, middle) the shifts are about 11 and 20 cm^{-1} for the A_{1g} and the E^1_{2g} mode, respectively. To gain deeper insight to the actual active material, the catalysts were also investigated by Raman spectroscopy after the catalytic tests. Despite excessive attempts (using laser lines at 514 nm, 633 nm or 1,064 nm) to record the according Raman modes of the ex situ activated catalyst after the HDS test, we were unable to detect. This leads to the conclusion, that the material undergoes severe changes under reaction conditions or during handling in air after the catalytic test. The first statement is in line with the observed induction period during the catalytic tests as discussed below.

Compared to the Raman bands of the bulk material the shape of the two modes of the catalysts are significantly different. It is well documented that the shape of the absorptions is strongly influenced by several materials properties: (a) a broad distribution of the stacking degree (thickness); (b) a variable size and shape of the platelets (either single or clustered) and (c) the presence of vacancies and other defects altering the size and planarity of the ordered domains inside the slabs. A clear cut between these factors cannot be performed. In any case, the Raman spectra of the two catalysts clearly evidence the nanosized nature of the MoS_2 slabs and in accordance with the results of X-ray diffraction and TEM experiments the defective nature of the slabs.

For each catalyst the rate constant was calculated from the DBT conversion as function of time, assuming that the DBT conversion is a pseudo-zero order reaction [14, 42], according to the equation:

$$X_{DBT} = \frac{1 - \eta DBT}{\eta DBT} = \left(\frac{k}{\eta DBT, 0}\right) t \qquad (2)$$

where X_{DBT} is the fraction of the DBT conversion, ηDBT = moles of DBT, k = pseudo-zero order rate constant, t = time in seconds and $(k/\eta_{DBT,0})$ is the slope. The mean standard deviation for catalytic measurements is about 2.5 %. The catalysts reported here required a distinct activation time in the reactor. Therefore, only the data after the activation period were used for the evaluation of the catalytic activities.

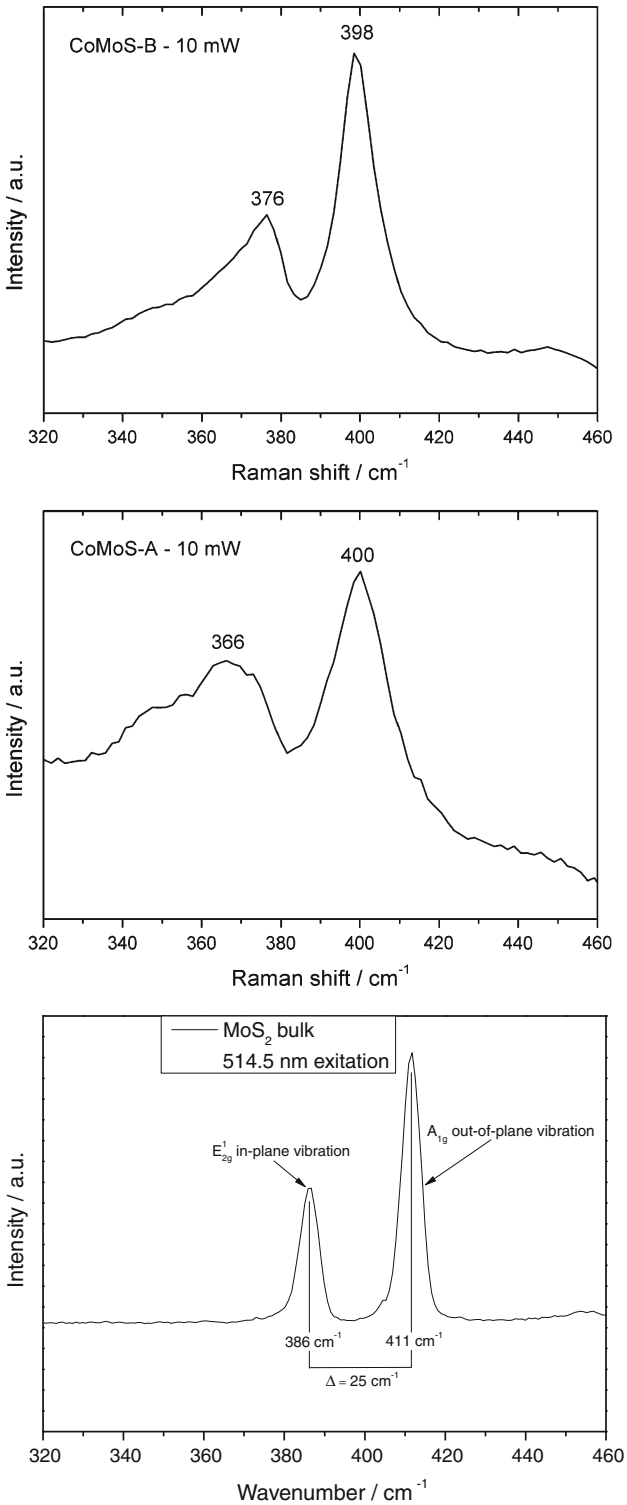

Fig. 5 Raman spectra of the ex situ activated catalyst (*top*), in situ activated catalyst (*middle*) and bulk MoS_2 (*bottom*)

Table 2 Gas chromatography analysis of HDS reaction products, HYD/DDS selectivity and kinetic data for the prepared catalysts

Catalyst	CHCPM (%)	DCH (%)	CHB (%)	BP (%)	THDBT (%)	DBT (%)	DBT (%) conversion	$\frac{[HYD]}{[DDS]}$	k × 10^6 (mol s^{-1} g^{-1})
CoMoS-A	1.73	3.52	14.18	34.79	5.20	40.56	59.43	0.15	2.75
CoMoS-B	0.89	3.18	18.36	61.42	1.04	15.09	84.91	0.02	4.11

The results of the catalytic tests are summarized in Table 2. Both catalysts prefer the DDS pathway with the in situ activated material showing almost twice the selectivity of the ex situ activated catalyst. The difference may be due to partial phase segregation as evidenced by the reflections of Co_9S_8 in the X-ray powder pattern of this catalyst. Such segregation of the promoter is not uncommon and was reported in several studies [4, 43–45]. The observed preference of the Co promoted catalysts for the DDS pathway is in accordance with previous literature reports [34].

The high rate constants for the two catalysts, 4.11 × 10^{-6} (CoMoS-B) and 2.75 × 10^{-6} [mol s^{-1} g^{-1} catalyst] (CoMoS-A) and the high DBT conversion percentage of 84.9 and 59.4 % after 5 h HDS reaction (Fig. 6) for the ex situ and in situ activated catalysts, respectively, both indicate very active catalysts. Compared to the rate constants and the conversion rates reported by Romero et al. [24] for a conventional MoS_2 catalyst obtained by thermal decomposition of ATM, and by Alvarez et al. for CoMoS catalysts [34], the present catalysts are significantly more active and exhibit higher conversion rates. The most active catalyst in the latter study was obtained from tetramethylammonium tetrathiomolybdate and $Co(NO_3)_2{\cdot}6H_2O$ as promoter source, showing a rate constant of 1.5 × 10^{-6} [mol s^{-1} g^{-1} catalyst] and 54 % DBT conversion after 5 h [34]. This catalyst was sulfur rich (S/Mo = 2.3) and also contained appreciable amounts of carbon (C/Mo = 2.1). The catalyst activated ex situ has a lower value for C:Mo of 1.39 before the HDS test and of 1.89 after the test reaction, while the S:Mo ratio is nearly identical with 2.28 and 2.33. The in situ activated material displays the highest ratios of 3.04 for S:Mo and 3.65 for C:Mo. In the present case the more active catalyst CoMoS-B has a significantly lower stacking and shorter MoS_2 layers lengths (see Fig. 3). An even lower stacking degree and also shorter layers were recently reported applying standard incipient wetness impregnation technique using ammonium heptamolybdate and Co nitrate [46].

There are some reports that Co promoted unsupported catalysts synthesized by decomposition of Mo thiosalts showed higher catalytic activities than similar catalysts prepared by other synthetic approaches [47]. Like for the catalyst CoMoS-A the thiosalt precursors are decomposed directly in an autoclave in the presence of a hydrocarbon solvent, and if a carbon containing thiosalt precursor is

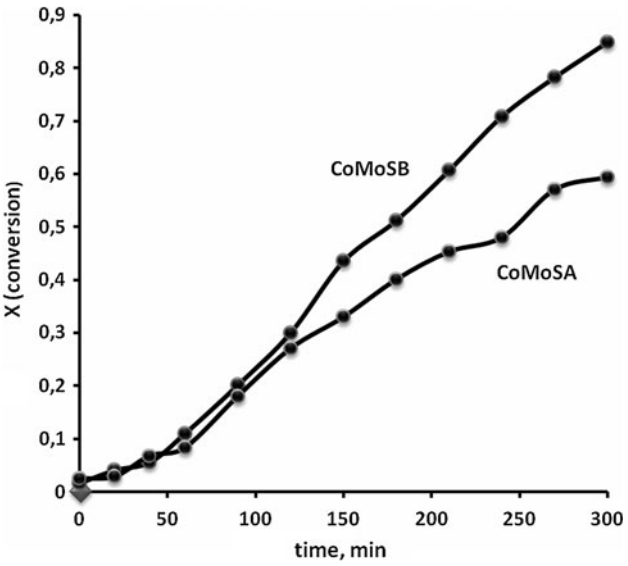

Fig. 6 Variation of the converted fraction of DBT Versus time, zero order

used an increase in the HDS activity was observed [48]. It is well documented that carbon has a beneficial effect on the activity of the catalysts. There are reports that a carbidic catalyst surface is formed when $(NR_4)_2MoS_4$ precursors are thermally decomposed [49]. Interestingly, an advanced carburization was observed on Co promoted catalysts [50]. The formation of MoS_xC_y phases was also observed and the results of the studies led to the conclusion that carbon participates directly in desulfurization reactions and do not act as simple spectator [11]. But it seems that only an optimal C content in the catalyst is beneficial and above this optimal concentration the catalyst becomes less active [24]. Hence, on the basis of all these findings it seems that ex situ decomposition of the precursor $Co(dien)_2MoS_4$ in combination with medium carbon containing TPATM yields a catalyst with a very good dispersion of Co, defective MoS_2 slabs with low stacking, short slabs and large amounts of CUS and edge-sites.

In the literature it was reported that the effect of the cobalt addition as promoter strongly depends on the method of activation and on the initial presence of alkyl groups in the sulphide precursors. A synergistic effect due to Co addition was only observed for ex situ activated catalysts (H_2/H_2S) in the absence of carbon in the thiosalt precursor, i.e., the promoting effect of Co is hindered by

carbon entities formed during the activation procedure [14]. For in situ prepared samples, carbon in the precursors is beneficial for the Co promoting effect [14, 48]. It is assumed that the beneficial role of carbon is due to structural effects leading to the formation of $MoS_{2-x}C_x$ phases with surface carbide-like species and/or to a better dispersion of the particles during the initial stages of the formation.

For the catalysts studied here the situation is quite different: the ex situ activated catalyst is significantly more active than the in situ activated material. The lower activity of the latter catalyst may be explained on the basis of a partial phase separation with Co_9S_8 formation. In addition, carbon and sulphur deposits on active sites of the catalyst may also play a role. Notice that in the case of the CoMoS-B catalyst the C/Mo ratio is lower compared to that of the CoMoS-A catalyst, with an excess of carbon yielding lower catalytic activity. Another important difference between the two catalysts is the heating rate applied during thermal decomposition. While the ex situ obtained catalyst was obtained heating the precursor with a rate of 1.66 °C/min., the in situ catalysts was prepared by a much higher heating rate of 60 °C/min. Hence, the more drastic conditions of the in situ approach may result in a type of sintering of the MoS_2 slabs (higher stacking degree) and a limited formation of the CoMoS phase.

4 Conclusions

The activation method in the formation of CoMoS-A (in situ) and CoMoS-B (ex situ) catalysts has not only a strong influence on their morphology and microstructure, but also on the development of catalytically active sites. SEM and TEM investigations revealed a pitched surface in CoMoS-A, while CoMoS-B possesses rather smooth surfaces. In accordance with the TEM investigations, Raman spectroscopy demonstrates a shorter stacking height in CoMoS-B. Both materials show high activity for the desulfurization with a pronounced activation behavior. The higher activity of CoMoS-B indicates a higher concentration of active sites where the sulfur can be adsorbed and a more pronounced synergistic effect due to the very good dispersion of the promotor atoms over the edges of the MoS_2 slabs forming a CoMoS phase.

Acknowledgments The authors appreciate the valuable technical assistance of Luis Lopez-Sosa and Isaac Velazquez Hernandez. Financial support by the German Science Foundation (DFG, BE 1653/32-1) is gratefully acknowledged.

References

1. Yoshimura Y, Yasuda H, Sato T, Kijima N, Kameoka T (2001) Appl Catal A Gen 207:303
2. Stanislaus A, Marafi A, Rana MS (2010) Catal Today 153:1
3. Pawelec B, Navarro RM, Campos-Martin JM, Fierro JLG (2011) Catal Sci Technol 1:23
4. Inamura K, Prins R (1995) Stud Surf Sci Catal 92:401
5. Lindner J, Villa Garcia MA, Sachdev A, Schwank J (1989) J Catal 120:487
6. Harris S, Chianelli RR (1986) J Catal 98:17
7. Toulhoat H, Kresse G, Raybaud P, Kasztelan S, Hafner J (1997) ACS Div Petrol Chem Prepr 42:114
8. Rodriguez JA, Liu P, Dvorak J, Jirsak T, Gomes J, Takahashi Y, Nakamura K (2003) Surf Sci 543:L675
9. Liu P, Rodriguez JA, Muckerman JT (2005) J Mol Catal A Chem 239:116
10. Chianelli RR, Berhault G, Torres B (2009) Catal Today 147:275
11. Kelty SP, Berhault G, Chianelli RR (2007) Appl Catal A Gen 322:9
12. Chianelli RR, Berhault G (1999) Catal Today 53:357
13. Yi Y, Zhang B, Jin X, Wang L, Williams CT, Xiong G, Su D, Liang C (2011) J Mol Catal A Chem 351:120
14. Poisot M, Bensch W, Fuentes S, Ornelas C, Alonso G (2007) Catal Lett 117:43
15. Huang Z-D, Bensch W, Kienle L, Fuentes S, Alonso G, Ornelas C (2008) Catal Lett 122:57
16. Huang Z-D, Bensch W, Kienle L, Alonso G, Fuentes S, Ornelas C (2008) Catal Lett 124:24
17. Huang Z-D, Bensch W, Kienle L, Fuentes S, Alonso G, Ornelas C (2009) Catal Lett 127:132
18. Huang Z-D, Bensch W, Kienle L, Alonso G, Bocarando J, Fuentes S, Ornelas C (2010) J Mol Catal A Chem 323:45
19. Poisot M, Bensch W, Fuentes S, Alonso G (2006) Thermochim Acta 444:35
20. Chianelli RR, Ruppert AF, Jose-Yacaman M, Vazquez-Zavala A (1995) Catal Today 23:269
21. Chianelli RR, Oil Gas Sci Tech–Rev IFP 61 (2006) 503
22. Chianelli RR, Pecoraro TA (1985) U.S. Patent 4, 528,089, to Exxon
23. Berhault G, Mehta A, Pavel A, Yang J, Rendon L, Yacamán MJ, Cota L, Duarte A, Chianelli RR (2001) J Catal 198:9
24. Romero-Rivera R, Camacho AG, Del Valle M, Alonso G, Fuentes S, Cruz-Reyes J (2011) Top Catal 54:561
25. Cruz-Reyes J, Avalos-Borja M, Farías MH (1989) Catal Lett 3:227
26. Perez de la Rosa M, Texier S, Berhault G, Camacho A, Yacaman MJ, Mehta A, Fuentes S, Montoya JA, Murrieta F, Chianelli RR (2004) J Catal 225:288
27. Berhault G, Perez de la Rosa M, Mehta A, Yacaman MJ, Chianelli RR (2008) Appl Catal A Gen 345:80
28. Joensen P, Frindt RF, Morrison SR (1986) Mat Res Bull 21:457
29. Liang KS, Chianelli RR, Chen FZ, Moss SC (1986) Non-cryst J Solids 79:251
30. Afanasiev P (2008) C R Chimie 11:159
31. Hagenbach G, Courty P, Delmon B (1971) J Catal 23:295
32. Hagenbach G, Courty P, Delmon B (1973) J. Catal 31:264
33. Alonso G, Berhault G, Aguilar A, Collins V, Ornelas C, Fuentes S, Chianelli RR (2002) J. Catal 208:359
34. Alvarez L, Espino J, Ornelas C, Rico JL, Cortez MT, Berhault G, Alonso G (2004) J Mol Catal A Chem 210:105
35. Lee C, Yan H, Brus LE, Heinz TF, Hone J, Ryu S (2010) ACS Nano 4:2695
36. Windom BC, Sawyer WG, Hahn DW (2011) Tribol Lett 42:301
37. Li Y, Wang H, Xie L, Liang Y, Hong G, Dai H (2011) J Am Chem Soc 133:7296
38. Ramakrishna Matte HSS, Gomathi A, Manna AK, Late DJ, Datta R, Pati SK, Rao CNR (2010) Angew Chem 122:4153
39. Frey GL, Tenne R, Matthews MJ, Dresselhaus MS, Dresselhaus G (1999) Phys Rev B 60:2883

40. Li X-L, Ge J-P, Li Y-D (2004) Chem Eur J 10:6163
41. Stacy AM, Hodul DT (1985) J Phys Chem Solids 46:405
42. Candia R, Clausen BS, Topsøe H (1982) J Catal 77:564
43. Koranyi TI, Paal Z (1990) Stud Surf Sci Catal 53:261
44. Candia R, Clausen BS, Topsøe H (1981) Bull Soc Chim Belg 90:1225
45. Yoosuk B, Kima JH, Song C, Ngamcharussrivichai C, Prasassarakich P (2008) Catal Today 130:14
46. Fuentes S, Diaz G, Pedraza F, Rojas H, Rosas N (1988) J Catal 113:535
47. Inamura K, Prins R (1994) J Catal 147:515
48. Jacobson AJ, Chianelli RR, Pecoraro TA (1987) US Patent 4,650,563
49. Seiver RL, Chianelli RR (1984) US 4,430,443 to Exxon
50. Berhault G, Cota Araiza L, Duarte Moller A, Mehta A, Chianelli RR (2002) Catal Lett 78:81
51. Daage M, Chianelli RR (1994) J Catal 149:414